Supplementary Information

Volumetric dried blood spot sampling by coordinated burst action of hydrophobic burst valves

Dries Vloemans[†1], *Lorenz Van Hileghem*[†1], *Wannes Verbist*[1], *Debby Thomas*[2], *Francesco Dal Dosso*[1], *and Jeroen Lammertyn*[*1]

[1]KU Leuven, Department of Biosystems - Biosensors Group, Willem de Croylaan 42, box 2428, 3001 Leuven, Belgium

[2]KU Leuven, Department of Pharmaceutical and Pharmacological Sciences, Herestraat 49, box 424, 3000 Leuven, Belgium

[†]These authors contributed equally to this work

*Corresponding author: jeroen.lammertyn@kuleuven.be; +3216321459

SI.1: Burst pressure calculation of HBVs and experimental setup

In Figure SI.1a-b, a schematic overview of the theoretical pressure profile with changing meniscus position in the HBV incorporated microfluidic channel is illustrated. A certain baseline pressure ($P_{c,1}$) is required to push the liquid at a constant flow rate through the non-treated channel with a contact angle $\theta_{c,1}$. Once liquid-air interface reaches the HBV it stops moving and an additional pressure is required to increase the surface area of the meniscus in order to meet the contact angle properties ($\theta_{c,2}$) of the local hydrophobic region. From the moment the applied pressure ($P_{c,2}$) is high enough so the contact angle of the meniscus meets the one of the hydrophobic coating, the liquid will be pushed through the HBV. Finally, when the meniscus reaches again the non-treated channel surface, the required pressure to maintain the flow rate drops again to its initial value ($P_{c,1}$) .

To calculate the burst pressure (ΔP_b) of the HBV, the measured pressure profile was first normalized by the average baseline pressure ($P_{c,1}$). This one was calculated as the average pressure value of the 10 second pressure profile before reaching the HBV. The burst pressure of the HBV was then calculated by taking the average pressure value over the time interval ($\Delta t = t_2 - t_1$) in which the liquid meniscus is moving over the HBV as is indicated in Figure SI.1b.

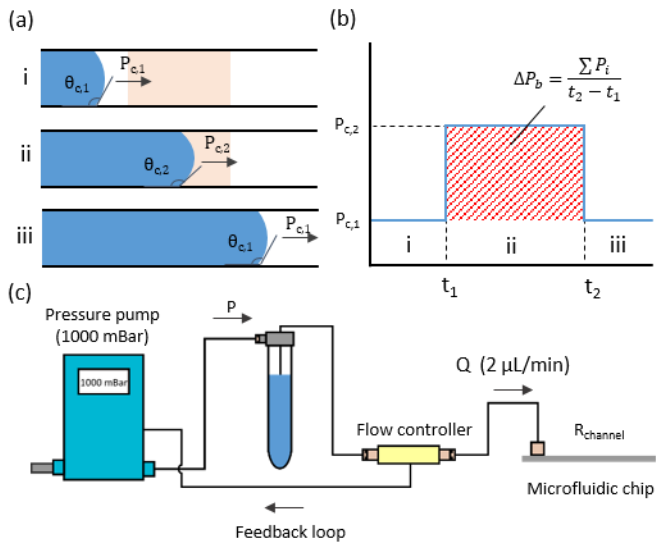

Figure SI.1 (a) Overview of the fluid meniscus position ([i] before, [ii] over, and [iii] after the HBV) within the channel. (b) Theoretical pressure profile to push a fluid front over the HBV. Average burst pressure is calculated as the average normalized pressure difference over the time interval t_2-t_1. (c) Schematic representation of the experimental measurement setup.

Liquid was injected in the microfluidic chips using pressure pumps (LINEUP FLOW EZ™ SERIES 1000 mBar, Fluigent, France). The experimental setup is illustrated in Figure SI.1c where a flow controller (Flow unit M, Fluigent, France) is used the control the injection flow rate precisely at 2 µL/min by controlling the applied pressure via a feedback loop system. The change in applied pressure and effective flow rate are recorded in real-time at a frequency of 0.1 Hz.

SI.2: Gravimetric methodology for the volumetric performance characterizations

A schematic of the experimental setup and the microfluidic design are illustrated in Figure SI.2a-b. Snapshots of different steps in the gravimetric volume characterization strategy are shown in Figure SI.2c. (i) An initial volume (20 µL) of citrated blood was preloaded via a prefilling hole in the microfluidic chip. Hereto, an extra hydrophobic barrier was implemented to direct the blood into the desired direction, avoiding it to flow toward the syringe pump connection. (ii) The sample plug was then pushed (15 µL/min) through the microfluidic network via a connected syringe pump. (iii) After volume metering the sample excess was discarded in the waste channel and (iv) finally the isolated metered sample volume was loaded on the circular filter paper. For this experiment, the device worked essentially as a non-integrated DBS system. This way, the filter paper, together with a supporting piece of PVC, can easily be removed from the chip in order to weigh the metered volume before and after sample loading.

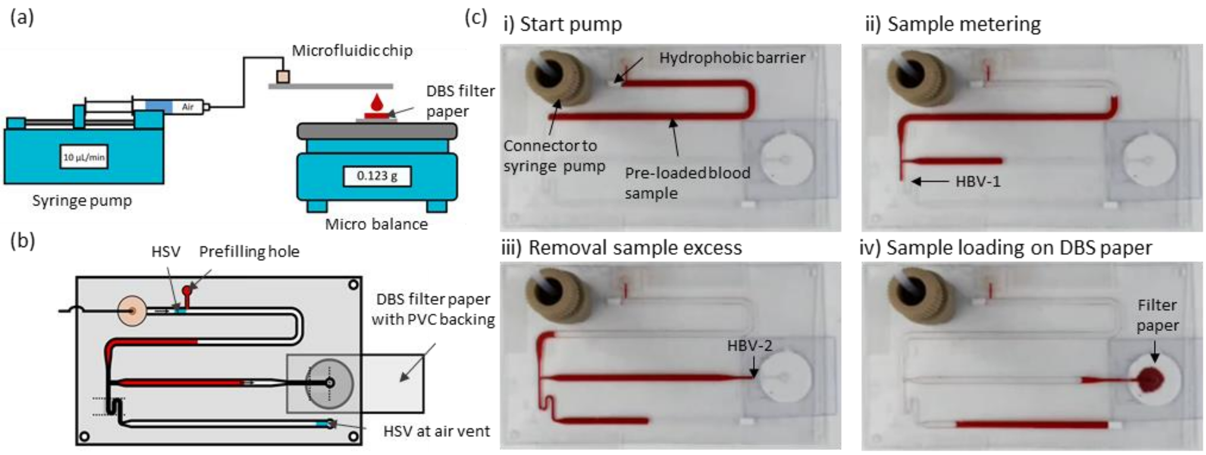

Figure SI.2 (a) Overview of the gravimetric measurement method. (b) Top view of the microfluidic device designed for these measurements. Below the metering outlet, a DBS filter paper is placed on top of a PVC backing for easy handling during weight measurements with the micro balance. c) Snapshots depicting the working principle of the gravimetric method to assess the accuracy, repeatability and Hct-independency of the metering system.

The accuracy and reproducibility of the gravimetric measurement method was evaluated by measuring the weight difference of paper substrates before and after application of a fixed volume of distilled water using a micropipette. Six repetitions were performed for the volumes of 5, 10 and 15 µL, for which the results are summarized in Figure SI.3. The measurements show a good reproducibility for each evaluated target volume (CV < 4%). Also, a strong agreement between the measured and target volumes (slope = 1) is observed, which confirms the good accuracy of the measurement method.

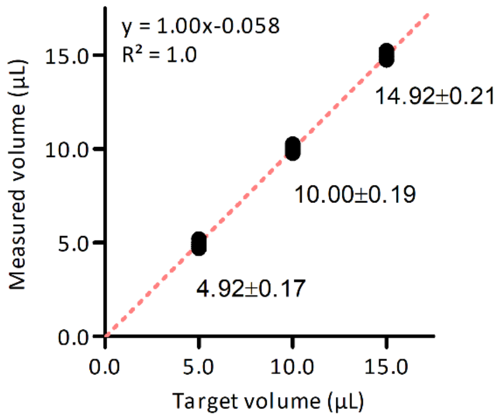

Figure SI.3: Reference gravimetric measurements with distilled water.

SI.3: Characterization of the burst pressures for different HBV types

Although the performed water contact angle measurements illustrated a good homogeneity of the coated surfaces, these measurements only give an indication of the surface properties on a relatively large scale. The required pressure to push the liquid over the hydrophobic treated zones in the channel is, however, only determined by the local surface properties of the coating at the meniscus interface of liquid. As a consequence, small artefacts in the coating might have a rather large influence on the burst pressure. It is expected that the local surface homogeneity of the Fluoropel coating is lower compared to the Aquapel solution as the solution contains silica nanoparticles which might cluster together upon evaporation of the solvent and this way introduce local artefacts. This hypotheses is reflected in the calculated differences between the measured and theoretical burst pressures given in Table SI.1. In particular, higher discrepancies can be observed for Fluoropel-based HBVs compared to Aquapel based ones.

Table SI.1: Theoretical and experimental obtained burst pressures for the different HBV types.

	Aq sc	**Fl sc**	**Aq dc**	**Fl + Aq**	**Fl dc**
$\Delta P_{b,\,theo}$ (Pa)	226	449	453	676	898
SD	29	33	58	62	67
$\Delta P_{b,\,exp}$ (Pa)	175	338	369	459	609
SD	26	57	25	37	60
$\Delta P_{b,\,theo}$- $\Delta P_{b,\,exp}$ (Pa)	52	111	83	217	289

Moreover, the performed contact angle measurements do not give any information on the patterning resolution and homogeneity of the coating at the edge of the hydrophobic region. The surface properties at the edge of the coating are, however, crucial in determining the burst pressure of the valve as at this interface the local change in contact angle occurs. In addition to this, due to the manual fabrication of the HBVs it can be expected that for dc HBV valves, the top and bottom coating are not perfectly aligned, what again can have an influence on the overall burst pressure. In general it is believed that by using an automated manufacturing process with a spray coating strategy, a clear reduction in the discrepancy can be achieved.

Another potential explanation for the observed discrepancy is the use of static instead of dynamic contact angles in the calculations of the burst pressure (Eq. (2) main manuscript). The bursting event of the HBV can be seen as a dynamic process in which the meniscus of the liquid has to change its interface to modify its contact angle from the non-treated PVC to meet the properties of the hydrophobic coated region. In general, the dynamic contact angle is smaller compared to the static one, what would result in overall lower burst pressures. The dynamic contact angle might also explain why a larger discrepancy between the theoretical and experimentally measured values was observed for HBVs in which the Fluoropel coatings are used. These coatings have superhydrophobic properties for which the difference between static and dynamic contact angles is almost negligible. As a consequence, the insertion of the dynamic contact angle in Eq. (2) of the main manuscript, only has an effect on the second term in brackets on the right hand side and not the first one, leading to a bigger difference in the burst pressure compared to when both terms are affected.

SI.4: Influence of microchannel dimensions on HBV burst pressure

According to Eq. (2) in the main text, the burst pressure of the HBV only depends on the height and not the width of the microchannel. This is because the mask-based coating strategy only alters the contact angle properties of the bottom or/and top of the microchannel while the contact angles of the side walls remain unchanged. To confirm this relation, the burst pressures of all five HBV configurations were also measured in 0.5 and 2.0 mm wide microchannels using the same methodology as described in the Section 2.4 of the Materials and methods. These burst pressures were then compared with the one of the 1.0 mm wide microchannels. A summary of these results is given in Figure SI.4a. Overall, the measured results confirm Eq. (2) as the burst pressures of each HBV configuration are within the same range for the different channel widths (see Tukey multiple comparison statistics in Table SI.2**Error! Reference source not found.**). However, in case of the dc HBVs a significant increase in burst pressure was observed for the 2.0 mm wide channels compared to the ones with a width of 0.5 and 1.0 mm.

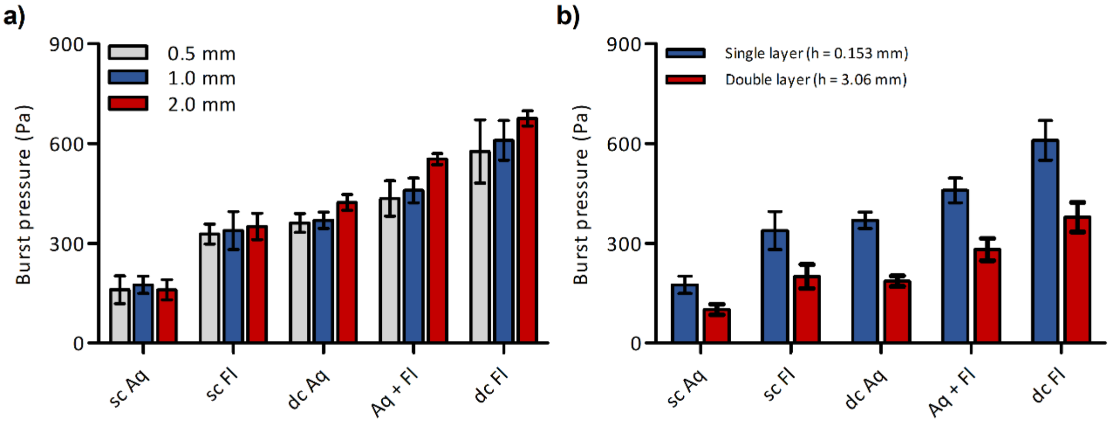

Figure SI.4: Average measured burst pressures of all HBV configurations for a) different channel widths of 0.5, 1.0 and 2.0 mm, and b) different channel heights of 0.153 and 0.306 mm. Error bars in a) and b) represent one standard deviation (n≥5).

This increase is not problematic in the context of this work as the dimensions of the microchannels, in which the HBVs are located, never exceed a width of 1.0 mm within our system. Moreover, when the trend in burst pressures for all HBV configuration is evaluated, the same 4 HBV configurations (even 5 for the 2.0 mm wide microchannels) show a significantly different burst pressure for each channel width (Table SI.3: Summary of Tukey multiple comparison statistics: overview of significantly different burst pressures between the five HBV configurations for each microchannel width.Table SI.3). As a consequence, we implemented the rule of thumb to use HBVs of the same width within the same microfluidic network.

Apart from the influence of the channel width, also the dependency of the channel height on the burst pressure was studied. Hereto, HBVs were made in microchannels consisting of a double PSA layer (0.306 mm thickness). As illustrated in Figure SI.4b, a clear drop in the measured burst pressure was observed what is in agreement with Eq. (2) of the main manuscript.

Table SI.3: Summary of Tukey multiple comparison statistics: overview of significantly different burst pressures between the evaluated channel widths (0.5, 1.0 and 2.0 mm) for each HBV configuration.

Sc Aq

LSMeans Differences Tukey HSD

α= 0.050 Q= 2.50434

LSMean[i]	Mean[i]-Mean[j] / Std Err Dif / Lower CL Dif / Upper CL Dif	LSMean[j] 0.5	1	2
0.5	Mean[i]-Mean[j]	0	-14.464	0.22397
	Std Err Dif	0	15.9308	16.5437
	Lower CL Dif	0	-54.36	-41.207
	Upper CL Dif	0	25.432	41.655
1	Mean[i]-Mean[j]	14.464	0	14.688
	Std Err Dif	15.9308	0	14.1085
	Lower CL Dif	-25.432	0	-20.645
	Upper CL Dif	54.36	0	50.0205
2	Mean[i]-Mean[j]	-0.224	-14.688	0
	Std Err Dif	16.5437	14.1085	0
	Lower CL Dif	-41.655	-50.021	0
	Upper CL Dif	41.2071	20.6445	0

Level		Least Sq Mean
1	A	174.78121
0.5	A	160.31719
2	A	160.09321

Levels not connected by same letter are significantly different.

Sc Fl

LSMeans Differences Tukey HSD

α= 0.050 Q= 2.64044

LSMean[i]	Mean[i]-Mean[j] / Std Err Dif / Lower CL Dif / Upper CL Dif	LSMean[j] 0.5	1	2
0.5	Mean[i]-Mean[j]	0	-10.724	-22.973
	Std Err Dif	0	27.2546	28.4665
	Lower CL Dif	0	-82.688	-98.137
	Upper CL Dif	0	61.2397	52.1909
1	Mean[i]-Mean[j]	10.7242	0	-12.249
	Std Err Dif	27.2546	0	27.2546
	Lower CL Dif	-61.24	0	-84.213
	Upper CL Dif	82.6882	0	59.7152
2	Mean[i]-Mean[j]	22.9729	12.2487	0
	Std Err Dif	28.4665	27.2546	0
	Lower CL Dif	-52.191	-59.715	0
	Upper CL Dif	98.1368	84.2126	0

Level		Least Sq Mean
2	A	350.47680
1	A	338.22811
0.5	A	327.50386

Levels not connected by same letter are significantly different.

Dc Aq

LSMeans Differences Tukey HSD

α= 0.050 Q= 2.58033

LSMean[i]	Mean[i]-Mean[j] / Std Err Dif / Lower CL Dif / Upper CL Dif	LSMean[j] 0.5	1	2
0.5	Mean[i]-Mean[j]	0	-7.8864	-61.381
	Std Err Dif	0	13.8212	15.4967
	Lower CL Dif	0	-43.55	-101.37
	Upper CL Dif	0	27.7769	-21.395
1	Mean[i]-Mean[j]	7.88641	0	-53.495
	Std Err Dif	13.8212	0	14.5896
	Lower CL Dif	-27.777	0	-91.141
	Upper CL Dif	43.5497	0	-15.849
2	Mean[i]-Mean[j]	61.3811	53.4947	0
	Std Err Dif	15.4967	14.5896	0
	Lower CL Dif	21.3946	15.8486	0
	Upper CL Dif	101.368	91.1407	0

Level			Least Sq Mean
2	A		422.71457
1		B	369.21989
0.5		B	361.33348

Levels not connected by same letter are significantly different.

Aq-Fl

LSMeans Differences Tukey HSD

α= 0.050 Q= 2.64044

LSMean[i]	Mean[i]-Mean[j] / Std Err Dif / Lower CL Dif / Upper CL Dif	LSMean[j] 0.5	1	2
0.5	Mean[i]-Mean[j]	0	-24.54	-119.19
	Std Err Dif	0	23.5337	24.5801
	Lower CL Dif	0	-86.679	-184.09
	Upper CL Dif	0	37.599	-54.289
1	Mean[i]-Mean[j]	24.5402	0	-94.651
	Std Err Dif	23.5337	0	23.5337
	Lower CL Dif	-37.599	0	-156.79
	Upper CL Dif	86.6793	0	-32.512
2	Mean[i]-Mean[j]	119.191	94.6513	0
	Std Err Dif	24.5801	23.5337	0
	Lower CL Dif	54.2893	32.5122	0
	Upper CL Dif	184.094	156.79	0

Level			Least Sq Mean
2	A		553.64547
1		B	458.99416
0.5		B	434.45397

Levels not connected by same letter are significantly different.

Dc-Fl

LSMeans Differences Tukey HSD

α= 0.050 Q= 2.64044

LSMean[i]	Mean[i]-Mean[j] / Std Err Dif / Lower CL Dif / Upper CL Dif	LSMean[j] 0.5	1	2
0.5	Mean[i]-Mean[j]	0	-33.695	-99.458
	Std Err Dif	0	41.6158	41.6158
	Lower CL Dif	0	-143.58	-209.34
	Upper CL Dif	0	76.1892	10.4257
1	Mean[i]-Mean[j]	33.6949	0	-65.764
	Std Err Dif	41.6158	0	43.4663
	Lower CL Dif	-76.189	0	-180.53
	Upper CL Dif	143.579	0	49.0066
2	Mean[i]-Mean[j]	99.4584	65.7635	0
	Std Err Dif	41.6158	43.4663	0
	Lower CL Dif	-10.426	-49.007	0
	Upper CL Dif	209.342	180.534	0

Level		Least Sq Mean
2	A	675.10689
1	A	609.34338
0.5	A	575.64851

Levels not connected by same letter are significantly different.

Table SI.2: Summary of Tukey multiple comparison statistics: overview of significantly different burst pressures between the five HBV configurations for each microchannel width.

0.5 mm

LSMeans Differences Tukey HSD

α= 0.050 Q= 2.95603

LSMean[i]	Mean[i]-Mean[j] / Std Err Dif / Lower CL Dif / Upper CL Dif	LSMean[j] Aq-Fl	Dc Aq	Dc Fl	Sc Aq	Sc Fl
Aq-Fl	Mean[i]-Mean[j]	0	73.1205	-141.19	274.137	106.95
	Std Err Dif	0	33.9975	33.9975	33.9975	35.5092
	Lower CL Dif	0	-27.377	-241.69	173.639	1.98384
	Upper CL Dif	0	173.618	-40.697	374.634	211.916
Dc Aq	Mean[i]-Mean[j]	-73.12	0	-214.32	201.016	33.8296
	Std Err Dif	33.9975	0	32.4154	32.4154	33.9975
	Lower CL Dif	-173.62	0	-310.14	105.196	-66.668
	Upper CL Dif	27.3771	0	-118.49	296.837	134.327
Dc Fl	Mean[i]-Mean[j]	141.195	214.315	0	415.331	248.145
	Std Err Dif	33.9975	32.4154	0	32.4154	33.9975
	Lower CL Dif	40.697	118.494	0	319.511	147.647
	Upper CL Dif	241.692	310.136	0	511.152	348.642
Sc Aq	Mean[i]-Mean[j]	-274.14	-201.02	-415.33	0	-167.19
	Std Err Dif	33.9975	32.4154	32.4154	0	33.9975
	Lower CL Dif	-374.63	-296.84	-511.15	0	-267.68
	Upper CL Dif	-173.64	-105.2	-319.51	0	-66.689
Sc Fl	Mean[i]-Mean[j]	-106.95	-33.83	-248.14	167.187	0
	Std Err Dif	35.5092	33.9975	33.9975	33.9975	0
	Lower CL Dif	-211.92	-134.33	-348.64	66.6891	0
	Upper CL Dif	-1.9838	66.6679	-147.65	267.684	0

Level					Least Sq Mean
Dc Fl	A				575.64851
Aq-Fl		B			434.45397
Dc Aq		B	C		361.33348
Sc Fl			C		327.50386
Sc Aq				D	160.31719

Levels not connected by same letter are significantly different.

1.0 mm

LSMeans Differences Tukey HSD

α= 0.050 Q= 2.89482

LSMean[i]	Mean[i]-Mean[j] / Std Err Dif / Lower CL Dif / Upper CL Dif	LSMean[j] Aq-Fl	Dc Aq	Dc Fl	Sc Aq	Sc Fl
Aq-Fl	Mean[i]-Mean[j]	0	89.7743	-150.35	284.213	120.766
	Std Err Dif	0	21.4229	24.0199	20.132	22.9021
	Lower CL Dif	0	27.7589	-219.88	225.934	54.4688
	Upper CL Dif	0	151.79	-80.816	342.491	187.063
Dc Aq	Mean[i]-Mean[j]	-89.774	0	-240.12	194.439	30.9918
	Std Err Dif	21.4229	0	22.614	18.4319	21.4229
	Lower CL Dif	-151.79	0	-305.59	141.082	-31.024
	Upper CL Dif	-27.759	0	-174.66	247.796	93.0072
Dc Fl	Mean[i]-Mean[j]	150.349	240.123	0	434.562	271.115
	Std Err Dif	24.0199	22.614	0	21.3951	24.0199
	Lower CL Dif	80.8161	174.66	0	372.627	201.582
	Upper CL Dif	219.882	305.587	0	496.497	340.648
Sc Aq	Mean[i]-Mean[j]	-284.21	-194.44	-434.56	0	-163.45
	Std Err Dif	20.132	18.4319	21.3951	0	20.132
	Lower CL Dif	-342.49	-247.8	-496.5	0	-221.73
	Upper CL Dif	-225.93	-141.08	-372.63	0	-105.17
Sc Fl	Mean[i]-Mean[j]	-120.77	-30.992	-271.12	163.447	0
	Std Err Dif	22.9021	21.4229	24.0199	20.132	0
	Lower CL Dif	-187.06	-93.007	-340.65	105.168	0
	Upper CL Dif	-54.469	31.0236	-201.58	221.725	0

Level					Least Sq Mean
Dc Fl	A				609.34338
Aq-Fl		B			458.99416
Dc Aq			C		369.21989
Sc Fl			C		338.22811
Sc Aq				D	174.78121

Levels not connected by same letter are significantly different.

2.0 mm

LSMeans Differences Student's t

α= 0.050 t= 2.05954

LSMean[i]	Mean[i]-Mean[j] / Std Err Dif / Lower CL Dif / Upper CL Dif	LSMean[j] Aq-Fl	Dc Aq	Dc Fl	Sc Aq	Sc Fl
Aq-Fl	Mean[i]-Mean[j]	0	130.227	-122.16	392.849	202.465
	Std Err Dif	0	16.8027	16.8027	14.6248	16.8027
	Lower CL Dif	0	95.6216	-156.77	362.728	167.859
	Upper CL Dif	0	164.833	-87.559	422.969	237.071
Dc Aq	Mean[i]-Mean[j]	-130.23	0	-252.39	262.621	72.2378
	Std Err Dif	16.8027	0	17.5498	15.4775	17.5498
	Lower CL Dif	-164.83	0	-288.54	230.745	36.0933
	Upper CL Dif	-95.622	0	-216.25	294.498	108.382
Dc Fl	Mean[i]-Mean[j]	122.165	252.392	0	515.014	324.63
	Std Err Dif	16.8027	17.5498	0	15.4775	17.5498
	Lower CL Dif	87.5593	216.248	0	483.137	288.486
	Upper CL Dif	156.771	288.537	0	546.89	360.775
Sc Aq	Mean[i]-Mean[j]	-392.85	-262.62	-515.01	0	-190.38
	Std Err Dif	14.6248	15.4775	15.4775	0	15.4775
	Lower CL Dif	-422.97	-294.5	-546.89	0	-222.26
	Upper CL Dif	-362.73	-230.74	-483.14	0	-158.51
Sc Fl	Mean[i]-Mean[j]	-202.47	-72.238	-324.63	190.384	0
	Std Err Dif	16.8027	17.5498	17.5498	15.4775	0
	Lower CL Dif	-237.07	-108.38	-360.77	158.507	0
	Upper CL Dif	-167.86	-36.093	-288.49	222.26	0

Level						Least Sq Mean
Dc Fl	A					675.10689
Aq-Fl		B				552.94189
Dc Aq			C			422.71457
Sc Fl				D		350.47680
Sc Aq					E	160.09321

Levels not connected by same letter are significantly different.

SI.5: Volumetric characterization of the metering system by a gravimetric method

The results of the gravimetric characterization of the volumetric performance are listed in Table SI.4. This is the summary of the results as depicted in Figure 5 and 6 of the main manuscript. Concerning the system accuracy, a slight increase in offset with the 10 µL target volume is observed for higher Hct levels (5.2% for 70% Hct level). However, when the offset of the average measured volumes for each Hct level is compared to the global average overall Hct levels (9.65 µL, which was plotted as the full red line in Figure 6), these differences reduce below 2%.

Table SI.4: Gravimetric measurements of the metering system its volumetric performance for different target volumes and varying Hct levels of blood samples.

Hct level (%)	Target volume (µL)	Average volume (µL)	SD	CV (%)
25	10	9.72	0.23	2.37
	5	4.86	0.15	2.99
40	10	9.79	0.22	2.22
	15	14.56	0.24	1.62
55	10	9.59	0.21	2.19
70	10	9.48	0.24	2.58

Although these results are highly promising, the volumetric performance could be further improved by i) replacing manual chip assembly and coating steps with an automated manufacturing process (i.e. roll-to-roll assembly and spray coating), ii) reducing the roughness of the channel walls by shifting to CO_2 laser cutting and iii) accounting for the volume loss and correcting by adjusting the location of the HBV within the metering channel.

SI.6: Multilayer configuration of SIMPLE-DBS sampling device, DBS loading, drying and removal

The multilayer configuration of the integrated SIMPLE-DBS device is illustrated in the cross-sections of Figure SI.5. A CF12 DBS paper is positioned underneath the distant part (after the dc HBV) of the metering channel which are in connection with each other via a sample loading hole. The top side of the metering channel is also foreseen with a hole at the same position of the sample loading hole. This punching hole is used for removing the dried DBS paper out of the chip before analysis by means of a pipet tip. During the sampling process, this hole is sealed with a removable film to prevent the intake of air. Likewise, a second removable film is attached to the bottom of the DBS paper. The metering system is in connection, via the DBS paper, with the bottom microfluidic layer in which the SIMPLE pumping mechanism is present which acts as the passive negative pressure source. In order to prevent the pulling of loaded blood sample out of the DBS paper in the connected microfluidic channel, a hydrophobic stop valve (HSV) is situated right next to the DBS paper.

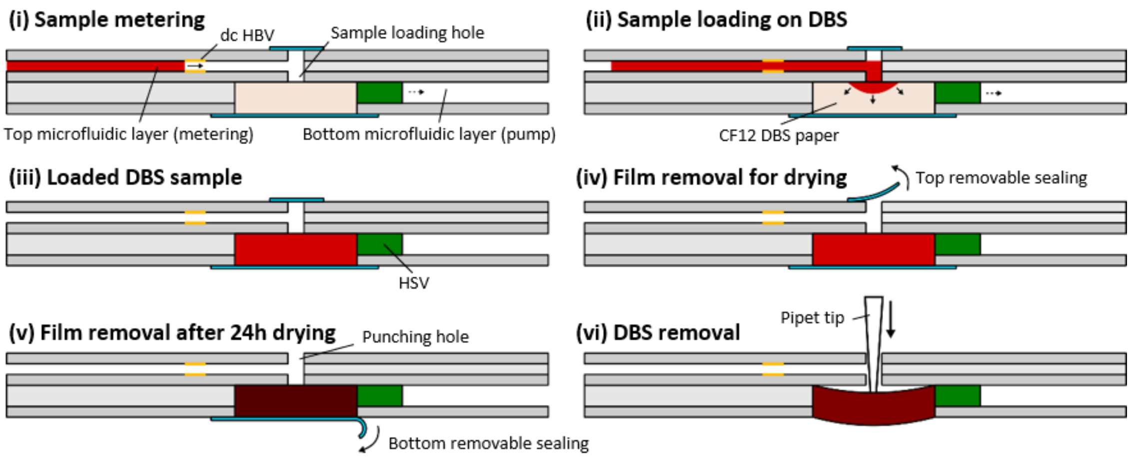

Figure SI.5: Cross-sections of the SIMPLE-DBS device illustrating the (i-iii) loading of the metered blood sample on the CF12 DBS paper, (iv) removal of the top sealing for a 24 h drying step and (v,vi) finally after peeling off the bottom sealing tape the DBS paper is pushed out of the chip by means of a regular pipet tip.

SI.7: ELISA measurements on extracted DBS samples

Table SI.5: Overview table of ELISA measurements on extracted DBS samples

DBS sample type	ADM conc. [µg/mL]	Loaded sample volume [µL]	ADM [µg/mL]	Stdev [µg/mL]	%CV	$ADM_{Measured}$ /ADM_{theor} conc. [%]
Whatman protein saver card - 6 mm sub-punch (gold standard)	0	40	**0.26**	0.02		
	1	40	**0.70**	0.11	15%	70%
	4	40	**2.67**	0.67	25%	67%
	16	40	**7.69**	0.23	3%	48%
			AVERAGE:		**15%**	**62%**
SIMPLE-DBS	0	9.65	**<0.03**	<0.03		
	1	9.65	**0.94**	0.08	8%	94%
	4	9.65	**3.28**	0.27	8%	82%
	16	9.65	**12.95**	2.15	17%	81%
			AVERAGE:		**11%**	**86%**
Whatman protein saver card – no sub-punch (whole spot analysis reference)	0	10	**<0.03**	<0.03		
	1	10	**0.77**	0.05	7%	77%
	4	10	**3.10**	0.50	16%	78%
	16	10	**12.71**	2.19	17%	79%
			AVERAGE:		**13%**	**78%**

SI.8: List of supplementary videos:

Video SI.1 – Working principle of the single metering system

Video SI.2 – Methodology of the gravimetric measurements

Video SI.3 – Working principle of the parallel metering system

Video SI.4 – Flow behaviour in the integrated SIMPLE-DBS system